Biogeosciences Discuss., 9, 15567–15602, 2012
www.biogeosciences-discuss.net/9/15567/2012/
doi:10.5194/bgd-9-15567-2012

Biogeosciences Discussions

UV/PAR radiations and DOM properties in surface coastal waters of the Canadian shelf of the Beaufort Sea during summer 2009

J. Para[1], B. Charrière[1], A. Matsuoka[2,3], W. L. Miller[4], J. F. Rontani[1], and R. Sempéré[1]

[1]Aix-Marseille Université, Mediterranean Institute of Oceanography (MIO), 13288, Marseille, Cedex 9; Université du Sud Toulon-Var, MIO, CNRS/INSU, MIO UMR7294, France
[2]Laboratoire d'Océanographie de Villefranche, Université Pierre et Marie Curie (Paris 6)/CNRS/INSU, B.P. 08, Port de la Darse, Villefranche-sur-Mer Cedex, 06230, France
[3]Joint International Laboratory, Université Laval (Canada) – CNRS (France), Département de Biologie and Québec-Océan, Université Laval, Pavillon Alexandre-Vachon 1045, avenue de la Médecine, Local 2078, G1V 0A6, Canada
[4]UGAMI/UGA Marine Science, Athens, GA 30602, USA

Received: 2 October 2012 – Accepted: 4 October 2012 – Published: 5 November 2012

Correspondence to: R. Sempéré (richard.sempere@univ-amu.fr)

Published by Copernicus Publications on behalf of the European Geosciences Union.

Abstract

Water masses from the Beaufort Sea in the Arctic Ocean were evaluated for dissolved organic carbon (DOC), and optical characteristics including UV and PAR diffuse attenuation (Kd), and chromophoric and fluorescent dissolved organic matter (CDOM and FDOM) as part of the MALINA field campaign (30 July to 27 August). Even with relatively low mean daily solar radiation incident on the sea surface (0.12 ± 0.03, 8.46 ± 1.64 and $18.09 \pm 4.20\,\mathrm{kJ\,m^{-2}}$ for UV-B (305 nm), UV-A (380 nm) and PAR, respectively), we report significant light penetration with 10 % irradiance depths ($Z_{10\,\%}(\lambda)$) reaching 9.5 m for 340 nm (UV-A) radiation in the Eastern sector and 4.5 m in the Mackenzie River influenced area (Western sector). Spectral absorption coefficients ($a_{\mathrm{CDOM}}(350\,\mathrm{nm})$ ($\mathrm{m^{-1}}$)) were significantly correlated to both diffuse attenuation coefficients (K_{d}) in the UV-A and UV-B and to DOC concentrations. This indicates CDOM as the dominant attenuator of UV solar radiation and suggests its use as an optical proxy for DOC concentrations in this region. Extrapolating CDOM to DOC relationships, we estimate that ~ 16 % of the DOC in the Mackenzie River does not absorb radiation at 350 nm. DOC and CDOM discharges by the Mackenzie River during the MALINA Cruise are estimated as ~ 0.22 TgC and 0.18 TgC, respectively. Three dissolved fluorescent components (C1–C3) were identified by fluorescence Excitation/Emission Matrix Spectroscopy (EEMS) and PARAFAC analysis. Our results showed an in-situ biological component (C1) that co-dominated with a terrestrial humic-like component (C2) in the Mackenzie Delta sector, whereas the protein-like (C3) component dominated in the saltiest waters of the North East sector.

1 Introduction

Even though the Arctic Ocean comprises only ~ 1 % of the Earth's total ocean volume and ~ 3 % of its surface area, it currently receives ~ 11 % of the global river runoff (Opsahl et al., 1999). Moreover, the effects of climate change are more pronounced

BGD
9, 15567–15602, 2012

toward the Earth's poles. Increasing air temperatures (+3 to 4 °C; IPCC, 2007) enhance numerous biogeochemical changes, particularly by affecting the integrity of the permafrost (Guo et al., 2007; Walvoord and Striegl, 2007). Approximately 50 % of the global terrestrial organic carbon pool is trapped in Arctic and sub-Arctic permafrost regions (Tarnocai et al., 2009) that are now warming (Foley, 2005). Therefore, increases in freshwater discharge coupled with changes in the mobility of terrestrial dissolved organic matter (DOM) are expected to increase DOM flux at high latitudes (Lawrence and Slater, 2005). This could lead to increased delivery of terrestrial DOM to the Arctic Ocean, as well as modified water circulation and sea ice coverage (Barber and Hanesiak, 2004).

Arctic rivers usually exhibit high organic matter content and low nutrient concentrations especially for nitrogen and phosphorus (Dittmar and Kattner, 2003). The DOM content in the Western Arctic region of the Beaufort Sea is strongly impacted by freshwater inputs from the Mackenzie River, which currently contributes the fourth largest freshwater discharge to the Arctic (Gordeev, 2006) and is the dominant source of terrestrial DOM to this region. River discharge, approximately 330 $km^3 yr^{-1}$ varies from 4000 $m^3 s^{-1}$ during winter (from December to May) to about 25 000 $m^3 s^{-1}$ during summer (from June to August) (e.g. O'Brien et al., 2006). The Mackenzie's flux of dissolved organic carbon (DOC) to the coastal Beaufort Sea is estimated to be ~ 1.04–1.76 TgC per year (Raymond et al., 2007).

The chromophoric fraction of DOM (CDOM) that absorbs solar irradiation over a broad range of ultraviolet (UV) and visible wavelengths is also delivered by the Mackenzie River. During the spring freshet and ice break up this increased amount of terrestrial CDOM in coastal areas can have numerous biological, chemical and physical effects. The presence of terrestrial CDOM decreases the euphotic depth for primary production, increases photooxidation (i.e. CO and CO_2 production) and increases mineralization of terrestrial DOC by stimulation of heterotrophic bacteria through the photo-production of labile organic substrates (Osburn et al., 2009). The combination of low sunlight intensity due to high solar zenith angles, large variations in seasonal

BGD
9, 15567–15602, 2012

day length, the influence of sea ice cover on sunlight penetration in surface waters, plume dynamics of the Mackenzie, and the changing DOM photochemical and biological reactivity in relation to season (Emmerton et al., 2008) all create a complex and highly variable photochemical environment over the Canadian shelf (Johannessen and Miller, 2001; Osburn et al., 2009). Consequently, in this Arctic environment that is so susceptible to the forcings of future climate change, better knowledge of the source, composition and surface distribution of CDOM, along with its effects on in situ optical characteristics is crucial to better quantify the processes involved in the organic carbon cycle in surface waters and at the land/sea interface.

Here, we report the spatial distribution of CDOM optical properties, in-air and in-water sunlight optical characteristics and their evolving patterns in surface coastal waters of the Canadian shelf of the Beaufort Sea during the summer of 2009. CDOM optical properties in sampled water, in combination of three-dimensional Excitation/Emission Matrix Spectroscopy (EEMS) with Parallel Factor Analysis (PARAFAC), was also examined to (i) define CDOM spectral absorbance features, (ii) identify and characterize the primary DOM fluorescent components and (iii) trace the corresponding spatial distributions of these signals in surface waters of the Canadian Arctic shelf.

2 Materials and methods

2.1 Study site and sample collection

Hydrological samples were collected from surface waters at 27 stations over the Canadian shelf of the Beaufort Sea onboard the research ice-breaker *CCGS Amundsen* during the Mackenzie Light and Carbon (MALINA) cruise held from 30 July to 27 August 2009 (Fig. 1). During this open water study period, the Mackenzie discharge was approximately 12 000 $m^3 s^{-1}$ (http://www.ec.gc.ca/rhc-wsc/) and the area investigated was characterized by an unusual ice cover extent and predominately overcast weather.

BGD
9, 15567–15602, 2012

Samples were collected using Niskin bottles equipped with Teflon O-rings and radiation in the Eastern sector contamination. For DOC determination, samples were directly transferred from the Niskin bottle through a Polycap AS75 (Whatman®) 0.2 µm nylon filter membrane cartridge into precombusted (6 h at 450 °C) glass ampoules, immediately acidified with 85 % H_3PO_4 (final pH ∼2) and flame sealed. Samples for CDOM and FDOM analysis were transferred from Niskin bottles into 10 % HCl-washed and precombusted (6 h at 450 °C) glass bottles and directly filtered in dim light through precombusted 0.7 µm GF/F filters, which had been pre-rinsed with Milli-Q water (Millipore®) water and with sample and then through 0.2 µm Nuclepore® polycarbonate filters that had been presoaked in 10 % HCl solution and rinsed with Milli-Q water and with sample according to the SeaWiFS protocols (Mueller and Austin, 1995). During sampling, in situ hydrological context (temperature and salinity vs. depth) was determined with a SeaBird Electronics 911 CTD profiler (Table 1).

2.2 Radiometric measurements

Duplicate in situ profiles of downward irradiance ($E_d(z,\lambda)$; µW cm^{-2} nm^{-1}) were performed, under mainly overcast skies, at 16 sampling stations (Fig. 1) using a Satlantic MicroPro® free-fall profiler equipped with OCR-504 irradiance sensors that measure the UV-B (305 nm), UV-A (325, 340 and 380 nm) and PAR (412, 443, 490 and 565 nm) spectral domains (Tedetti et al., 2009). Surface irradiance ($E_s(\lambda)$ in µW cm^{-2} nm^{-1}) was simultaneously measured at the same wavebands on the ship's roof with matching OCR-504 sensors to account for variations in the sky conditions during the cast as well as to monitor UV and PAR solar irradiance during the day. For both the in-water and in-air OCR-504 sensors, the Full-Width Half-Maximum (FWHM) was 2 nm for the 305, 325 and 340 nm channels and 10 nm for the PAR channels. The MicroPro® free-fall profiler, equipped with pressure, temperature and tilt sensors, was deployed from

BGD
9, 15567–15602, 2012

the front of the ship and profiled ~50 m away to minimize shadowing effects and disturbances.

Each cast was accompanied by a measurement of the dark current (instrument on deck) and a pressure tare (instrument at sea surface). To obtain as many valid measurements as possible (i.e. tilt $< 5^{\circ}$), the profiler was nose ballasted to provide a descent rate of ~70 cm s^{-1} at a sampling rate of 7 Hz (i.e., sampling resolution of 10 cm). Measurements were logged using Satlantic's Satview® 2.6 software. The latter allowed for initial data processing, such as channel integration for PAR calculations, radiometric calibration, dark correction, pressure tare application and the removal of data with tilt $< 5^{\circ}$. Satview®'s data interpolation option was not used, choosing rather to work with the raw radiometric data for Kd calculations. Profiles of downwelling irradiance in the total PAR range were calculated by Prosoft Satlantic software from the four PAR channels.

The diffuse attenuation coefficients for downwelling UVR and PAR irradiances (K_d (λ) m^{-1}) were calculated, assuming a homogeneous surface mixed layer, as the slope of the best fit linear regression for the log-transformed downwelling irradiance data vs. depth relationship defined by the equation:

$$E_d(z,\lambda) = E_d(0^-,\lambda)\exp^{(-K_d(\lambda)z)} \quad (1)$$

E_d (0^-, λ), the downwelling irradiance just beneath the sea surface, was computed from above-water deck irradiance measurements, E_d (0^+, λ), using the theoretical relationship defined by Smith and Baker (1984):

$$E_d(0^-,\lambda) = E_d(0^+,\lambda)/(1+\alpha) \quad (2)$$

where α is the ocean surface albedo (OSA) determined using a "look up table" (Jin et al., 2004; http://snowdog.larc.nasa.gov/jin/getocnlut.html) based on the validated Coupled Ocean-Atmosphere Radiative Transfer (COART) model. Three of the 4 model parameters (SZA, cloud optical depth and wind speed) required to retrieve α

BGD
9, 15567–15602, 2012

at any band of the solar spectrum are reported in Table 2 for our stations. The fourth required parameter, chlorophyll *a* concentration, was set at a value of 0.1 µg l^{-1} for all stations (S. Bélanger, personal communication, 2012). Accordingly, mean α values at 305, 325, 340, 380 nm and PAR were 0.062 ± 0.005, 0.062 ± 0.005, 0.065 ± 0.006, 0.069 ± 0.008 and 0.055 ± 0.001, respectively. Because attenuation in natural waters is known to decrease with increasing wavelength in the UV range, any $K_d(\lambda)$ value that was lower than those at longer wavelengths was deleted. Values of $K_d(\lambda)$ at 305 nm were particularly prone to error. The mean variability (CV %) of K_d(UV) and K_d(PAR) determined between duplicate profiles was within 3 %.

2.3 DOC analysis

The Shimadzu instrument used in this study is the commercially available model TOC-5000 Total Carbon Analyzer with a quartz combustion column filled with 1.2 % Pt on silica pillows with modifications previously described in Sohrin and Sempéré (2005). The accuracy and the system blank of our instrument were determined by the analysis of seawater reference material (Hansell, D., Rosenstiel School of Marine and Atmospheric Science, Miami, USA), including Deep Atlantic Water (DAW) and Low Carbon Water (LCW) reference standards. The average DOC concentrations in the DAW and in the LCW reference standards were 45 ± 2 µM C (n = 24) and 1 ± 0.3 µM C (n = 24), respectively. Carbon levels in the LCW ampoules were similar to and often higher than the Milli-Q water produced in our laboratory. The nominal analytical precision for the procedure was less than 2 %.

2.4 CDOM optical properties

2.4.1 Absorbance measurements

After collection and filtration of the samples, CDOM absorbance (280–700 nm) was measured onboard (within 24 h) using a multiple pathlength, liquid core Ultrapath

BGD
9, 15567–15602, 2012

waveguide system (MPLCW; WPI Inc.). The detailed methodology for determining light absorbance of CDOM (280–735 nm) using this system is documented in Matsuoka et al. (2012). Spectral absorption coefficients, $a_{CDOM}(\lambda)$ (m^{-1}) were obtained using the following relationship :

$$a_{CDOM}(\lambda) = 2.303A(\lambda)/L \quad (3)$$

where $A(\lambda)$ (dimensionless) is the absorbance at wavelength λ (nm) and L is the pathlength in meters. The value of the spectral slope coefficient for the CDOM spectrum (S_{CDOM}) was determined by fitting a non-linear exponential regression to the original $a_{CDOM}(\lambda)$ data over the 350–500 nmspectral range (Babin et al., 2003; Matsuoka et al., 2011, 2012).

2.4.2 Fluorescence measurements

For fluorescence measurements, samples were stored in the dark at 4 °C, transported to the laboratory and analyzed in the Mediterranean Institute of Oceanography by MIO within 3 months of sampling. Samples were transferred to a 1 cm pathlength far UV silica quartz cuvette (170–2600 nm; LEADER LAB), thermostated at 4 °C and analyzed with a Hitachi (Japan) Model F-7000 spectrofluorometer. Instrument settings, measurement protocol and spectral correction procedures are fully described in Tedetti et al. (2010) and Para et al. (2011). Briefly, the spectral correction for the instrumental response was conducted according to the procedure recommended by Hitachi (Hitachi F-7000 Instruction Manual). First, the excitation (Ex) instrumental response was obtained by using a Rhodamine B standard and a single-side frosted red filter in the Ex scan mode. The emission (Em) calibration was performed with a diffuser in synchronous scan mode. The Ex and Em spectra obtained over the range 240–550 nm were applied internally as the instrument blank to correct subsequent spectra.

EEM spectra were generated using Ex wavelengths from 240 to 550 nm (5 nm intervals), Em wavelengths from 300 to 550 nm (2 nm intervals), a scan speed of 2400 nm min^{-1} and 5 nm bandwidths (Full-Width Half-Maximum; FWHMs) for both

BGD
9, 15567–15602, 2012

Ex and Em. Milli-Q water was analyzed to allow all fluorescence data (blanks, standards, samples) to be normalized to the intensity of the Raman scatter peak at Ex/Em: 275/303 nm (5 nm bandwidths) (Coble et al., 1993; Coble, 1996; Belzile et al., 2006). Solutions of quinine sulfate (Fluka) in 0.05 M H_2SO_4 (1–10 ppb) were also analyzed and FDOM data were converted into quinine sulfate units (QSU) to further normalize fluorescence results and to allow comparison to previously published work.

The complex mixture of fluorophores that contribute to the total FDOM signal was then statistically decomposed into its primary components using the PARAFAC statistical tool based on an alternating least square (ALS) algorithm (Stedmon et al., 2003). The analysis was carried out in MATLAB 7.1 with the DOMFluor toolbox (Stedmon and Bro, 2008), freely downloadable from the Chemometrics site at the University of Copenhagen (www.models.life.ku.dk). Implementation of the toolbox for our data set followed protocols presented in Stedmon and Bro (2008). A three-component PARAFAC model was validated using split-half analysis (Stedmon et al., 2003) and provided low residual values when compared to EEM spectra obtained from the original samples, thus confirming the model's ability to extract the majority of the samples' fluorescent features and appropriately characterize the surface FDOM composition for this area.

3 Results and discussion

3.1 Surface irradiance at sea surface and diffuse attenuation coefficient of light in surface waters

During the MALINA cruise, the mean daily doses (kJ m^{-2}) of UV-B (305 nm), UV-A (380 nm) and PAR incident on the sea surface were 0.12 ± 0.03, 8.46 ± 1.64 and 18.09 ± 4.20 kJ m^{-2}, respectively. These mean daily doses were low and relatively constant throughout the study period due to the presence of persistent clouds that reduced the overall incident solar radiation and particularly the UV-B. Such daily doses for UV-B (305 nm), UV-A (380 nm) and PAR (490 nm) were 10-, 2- and 1.5-fold lower,

BGD
9, 15567–15602, 2012

respectively, than that received at the sea surface in the south Pacific gyre during (austral) summer cloudy days (Sempéré et al., 2008).

The UV-B K_d (305 nm) values in the North East sector averaged $0.380 \pm 0.055\,m^{-1}$. Because the overall Es (UV-B) was notably weak, the determination of Kd (UV-B) for approximately 50 % of the stations sampled was not possible, particularly for the 'organic-rich stations' located mostly in the vicinity of the Mackenzie Delta (salinity ≤ 25; Table 2). Consequently, K_d (305 nm) is not discussed extensively in the following section. However, it is interesting to notice that K_d (305 nm) values are in the range of those reported for other marine areas including Arctic Baffin Bay ($0.58\,m^{-1}$), Antarctic waters ($0.29–1.15\,m^{-1}$) and the Mediterranean Sea ($0.14–0.92\,m^{-1}$) but significantly lower than those reported for Arctic Sammanger fjord ($1.91–3.8\,m^{-1}$) (Tedetti and Sempéré, 2006). For reference, the lowest K_d (305 nm) values ever recorded in the surface ocean ($0.083\,m^{-1}$) were reported for the center of the East Pacific Gyre (Tedetti et al., 2007).

$K_d(\lambda)$ values determined in both the UV-A and PAR (Table 2) spectral domains showed strong variation among the 16 sampling stations monitored (Fig. 2). Maximum K_d (UV-A) and K_d (PAR) values were observed in the North West and North East sectors at stations 670 (closest station to the Mackenzie Delta) and 170 (Cape Bathurst area; Fig. 1), respectively. Minimum K_d (UV-A) and K_d (PAR) values were observed at stations 345–360 and 460, respectively (Table 2). In the North West sector, the mean K_d (UV-A) at 325, 340 and 380 nm and K_d (PAR) values were 1.268 ± 0.383, 1.055 ± 0.318, 0.512 ± 0.2145 and $0.136 \pm 0.025\,m^{-1}$, respectively, while the corresponding values in the saltiest sector (North East sector; salinity > 25) were approximately 2.5- and 1.5-fold lower for UV-A and PAR, respectively (Fig. 3; Table 2). Just as was discussed for K_d (305 nm) above, Kd values for UV-A and PAR are also in the range of those reported for other marine areas including Arctic and Antarctic waters ($0.29–1.15\,m^{-1}$) and the Mediterranean Sea ($0.14–0.92\,m^{-1}$) (Tedetti and Sempéré, 2006).

The weak solar UV intensity measured at the sea surface suggests that there was a limited amount of in situ photochemical degradation involving CDOM during the

BGD
9, 15567–15602, 2012

MALINA cruise, regardless of solar radiation penetration depth. Regardless, the 10 % irradiance depth, ($Z_{10\%}(\lambda)$ in m), defined as the depth where the downward irradiance is 10 % of its surface value ($Z_{10\%}(\lambda) = 2.3/K_d(\lambda)$), in the North East sector had a mean $Z_{10\%}(305)$ value of 6 m with this value reaching 9.5 m for $Z_{10\%}(340)$ (Station 540). In the Mackenzie influenced area (Western sector), $Z_{10\%}(305)$ may still reach 4.5 m which can be considered a significant depth for photochemical reactions in this riverine setting.

During the relatively moderate Mackenzie discharge (12 000 $m^3 s^{-1}$; Carmack and Macdonald, 2002) observed during the study period, the significant contribution of terrestrial CDOM was expected to control the overall spatial distribution of both K_d (UV-A) and K_d (PAR) values on the Canadian shelf and should correlate with the surface salinity gradients induced by the Mackenzie's plume. Indeed, in the North West sector both K_d (UV-A) and K_d (PAR) increased with lower salinity, whereas values remained roughly constant or slightly increased for salinity higher than 28 in the North East sector (Fig. 3; Table 2). The downwelling attenuation of both UV-A and PAR in the North West sector appeared to be mainly controlled and strongly impacted by CDOM and particles carried by the Mackenzie plume, while in the saltiest surface waters (North East sector) other CDOM sources (primary production, CDOM production by bacterioplankton) appeared to have the ability to increase attenuation of both UV-A and PAR almost as strongly as the river plume.

3.2 DOM characteristics

3.2.1 Chromophoric DOM

The overall DOM characteristics varied greatly among the three surface water salinity sectors observed for the Canadian shelf during the summer of 2009 (Figs. 4–5; Table 1). Surface mean DOC concentrations increased from 71 ± 15 µM C in the North East sector (salinity ≥ 25) to 106 ± 45 and 310 ± 87 muM C in the North West (15 < salinity < 25) and Mackenzie Delta (salinity < 15) sectors, respectively (Fig. 4).

BGD
9, 15567–15602, 2012

Surface mean DOC and $a_{CDOM}(350)$ values in the Mackenzie Delta sector were up to 4 and 20 times higher, respectively, than in the saltiest surface waters (North East sector; Table 1). In the Mackenzie Delta and North West sectors (salinity < 25), both $a_{CDOM}(350)$ and DOC values decreased linearly with salinity. These co-trending relationships with the surface salinity gradient (Fig. 6) highlight the fact that in surface waters, during the study period, $a_{CDOM}(350)$ was a good proxy for DOC in the Mackenzie dilution plume area (Fig. 6). Matsuoka et al. (2012) observed a similar relationship between DOC content and $a_{CDOM}(440)$. Although, the correlation between DOC and $a_{CDOM}(350)$ is less significant for the saltiest waters of the North East sector (salinity ≥ 25), $a_{CDOM}(350)$ remained an acceptable proxy for DOC (Fig. 6).

Based on the $a_{CDOM}(350)$ and DOC distributions alone, it appears that the origin of DOM in each region is shifted throughout the shelf system. In the Mackenzie Delta and North West sectors (salinity < 25), the origin of the DOM appears to be mostly allochthonous and reflects the mixing process of the Mackenzie's terrestrial input, while in the saltiest surface waters (North East sector), autochthonous DOM appears to dominate. Sea ice formation/brine rejection and upwelling processes are common physical features in this salty area and have the capacity to both deliver new DOM and enhance surface in situ production of DOM (Carmack and Macdonald, 2002; Barber and Hanesiak, 2004; Guéguen et al., 2007; Walker et al., 2009; Mucci et al., 2010). Additional CDOM could be produced by zooplankton and bacterioplankton communities (Nelson et al., 2004). DOM introduced by either process could have the capacity to create the attenuation patterns for both UV-A and PAR seen in Fig. 3. An upwelling event close to the Cape Bathurst area (Fig. 1) was clearly identified during our sampling period and has been previously observed by Mucci et al. (2010). It enhanced primary production in the surface waters surrounding Cape Bathurst, manifested as the overall highest surface chlorophyll *a* concentrations (~ 7 µg l^{-1}) observed at station 170 (S. Bélanger, personal communication, 2012). Subsequent organic by-products from this productive area could explain the high values for DOC, $a_{CDOM}(350)$ and K_d (UV-A and PAR) observed at this station (Tables 1 and 2).

BGD
9, 15567–15602, 2012

In general, these results suggest both allochthonous and autochthonous origins for DOM in the surface waters of the Canadian Shelf. An additional feature of the source material can be seen in the estimation of the optically inactive fraction of the DOC pool in the study area. Using the y-intercept in Fig. 6 (i.e. $a_{CDOM}(350) = 0\,m^{-1}$) 63.8 µM of DOC do not absorb radiation at 350 nm in the Mackenzie River. Such results indicated that, on average, ~16 % of the DOC are optically inactive at 350 nm in the Mackenzie River, being in line with a_{CDOM} (440) Matsuoka et al. (2012) results. Based on a carbon content of ~400 µM C in the river mouth (Table 1) the DOC discharge by the Mackenzie River can be estimated, during the MALINA Cruise (30 July–27 August) to approximately 0.22 TgC (i.e. 10 to 20 % of annual DOC fluxes and 6 to 10 % of annual TOC fluxes, Raymond et al., 2007; MacDonald et al., 1998). Considering that ~64 µM C does not absorb radiation in the UV (Fig. 6), CDOM discharge can be estimated to be 0.186 TgC. Previous study showed comparable discharge for particulate and dissolved organic carbon on an annual basis (Macdonald et al., 1998; Dittmar and Kattner, 2003).

K_d (UV-A) and K_d (PAR) in the North West and North East sectors (i.e., at salinity > 20; where radiometric measurements were performed) were significantly correlated to a_{CDOM} (350) values (Fig. 7) except for the single K_d (PAR) value observed at station 170 (Fig. 7) where the highest chlorophyll-a content occurred (7 µg l^{-1}, data not shown and $a_{CDOM}(350) = 0.56\,m^{-1}$). Interestingly, the y-intercept values of these relationships (Fig. 7) were in the range of attenuation coefficient values found for pure water, $K_w(\lambda)$, determined by Baker and Smith (1982). Therefore, it can be argued that CDOM is the dominant attenuator for not only UV-A radiation, but also for PAR. This is in good agreement with Retamal et al. (2008) and their report of control of PAR-light absorbance by CDOM in the Beaufort Sea.

The spatial evolution of S_{CDOM} values and the specific absorption coefficient at 350 nm, a_{CDOM} (350), (calculated as a_{CDOM} (350)/DOC; Table 2) are both expected to change to reflect DOM origin and chemical structure and should reinforce the hypothesis of a restricted spatial dominance of the allochthonous DOM in the Mackenzie Delta sector (salinity < 15). Interestingly, during the MALINA study period there was no

BGD
9, 15567–15602, 2012

significant difference among mean S_{CDOM} values for each salinity sector (Table 1) despite the relative scatter of S_{CDOM} values observed at salinity > 25 (Fig. 5c). This could be attributed to the high S_{CDOM} values determined for the allochthonous CDOM of the Mackenzie Delta sector ($S_{CDOM} = 0.019 \pm 0.001\,nm^{-1}$) that are more typical of marine CDOM thus preventing a clear spatial contrast in S_{CDOM} values throughout the system. However, the high S_{CDOM} values for the Mackenzie Delta sector are similar to values previously reported for CDOM from the Mackenzie River during summer (Retamal et al., 2007; Osburn et al., 2009; Stedmon et al., 2011). Stedmon et al. (2011) and Osburn et al. (2009) attributed these high S_{CDOM} values to preferential adsorption by high molecular weight, hydrophobic DOM components of the abundant suspended sediments as well as more extensive photodegradation of the high molecular weight fraction in the important Mackenzie watershed. Interestingly, a_{CDOM} (350) values which can be used as a proxy of terrestrial/aromatic CDOM in the DOC pool (Belzile et al., 2002; Gareis et al., 2010), were 5–6 times higher ($15.24 \pm 1.84\,m^2\,\mu mol^{-1}$) in the Mackenzie Delta sector than in the North East sector ($2.71 \pm 0.86\,m^2\,\mu mol^{-1}$).

3.2.2 Fluorescent DOM – fluorescent component characteristics

Three fluorescent components (Fig. 8) were identified with PARAFAC analysis using a total of 54 EEM spectra collected from surface waters and the deep chlorophyll maximum (DCM) for the 27 stations investigated during the MALINA cruise. Excitation/Emission (Ex/Em) maxima wavelengths of the three components are presented in Table 3 and compared to recent Arctic and sub-Arctic studies (Stedmon et al., 2007; Walker et al., 2009; Fellman et al., 2010). The Ex/Em maxima of component 1 (C1) are close to the marine humic-like (M peak) proposed by Coble (1996) and has been reported to be a ubiquitous component derived from the microbial degradation of phytoplankton by-products (Nagata, 2000; Stedmon and Markager, 2005; Zhang et al., 2009) and from specific Arctic terrestrial sources at low salinity (Walker et al., 2009). Component 2 (C2) presents a similar pattern to peaks A and C of Coble et al. (1998) and have been previously associated with high molecular weight and aromatic terrestrial organic

BGD
9, 15567–15602, 2012

matter (Stedmon et al., 2003; Walker et al., 2009). The low Ex/Em maxima of C3 are comparable to protein-like components previously observed in surface waters of fresh and marine systems (Coble, 1996; Yamashita et al., 2003; Para et al., 2010).

Our results showed that the C1 and C2 components are significantly correlated with both salinity (negative linear correlation) and $a_{CDOM}(350)$ (positive linear correlation) in the Delta and North West sectors (Figs. 9–10). Interestingly, at higher salinity ($S \geq 25$, North-East sector) the correlations are no longer observed. The C3 component did not exhibit any correlation with either salinity or $a_{CDOM}(350)$. In the North East sector (salinity > 25), the relative contribution of fluorescent components was clearly dominated by the protein-like C3 (57 ± 7 %), followed by the ubiquitous humic-like C1 (30 ± 4 %) and the terrestrial C2 (13 ± 4 %), respectively. In surface waters of the North West sector (15 < salinity < 25), we observed a co-dominance of both C1 (40 ± 8 %) and C3 (40 ± 13 %) while the relative contribution of the terrestrial component C2 was around two times lower (20 ± 6 %). In the Mackenzie Delta sector (salinity < 15), the relative contribution of the in-situ biological component C1 (52 ± 2 %) and terrestrial component C2 (36 ± 6 %) reached their highest contribution, while C3 (12 ± 7 %) was around 5 times lower than the same component determined for the saltiest surface waters.

Therefore, during our study period, the FDOM content in surface waters of the Canadian shelf was strongly influenced by allochthonous DOM that originated from the Mackenzie, except in the saltiest waters where autochthonous in-situ biological FDOM prevailed. Surprisingly, the allochthonous fluorescent DOM carried by the Mackenzie into the Beaufort Sea presents both a terrestrial humic and a in-situ biological signature. Indeed, the fluorescence intensity of the in-situ biological component C1 co-dominated with the terrestrial humic-like component C2 in controlling the overall allochthonous fluorescent DOM pool of the Mackenzie Delta sector. Interestingly, the overall distribution of the terrestrial component C2 appeared restricted to the Mackenzie Delta sector and correlated well with the strongly absorbing allochthonous DOM observed, while the

BGD
9, 15567–15602, 2012

surface distribution of the in-situ biological component C1 appeared more widespread in the whole system.

The Mackenzie Delta is composed of numerous (~ 45 000) shallow (1.6 m depth on average) macrophyte-rich lakes (Emmerton et al., 2007; Squires et al., 2009) that significantly influence the Mackenzie DOM content prior to its marine discharge in summer (Emmerton et al., 2008; Gareis et al., 2010). In addition, macrophyte and phytoplankton degradation/exudation processes in fresh shallow (Zhang et al., 2009) and marine systems can lead to the production of a marine humic-like fluorescent component (M peak; Coble, 1996) comparable to our C1. Therefore, the strong in situ biological fluorescent DOM fraction observed in the Mackenzie Delta sector during this study may partly originate from strong biological activity (Squires et al., 2009) occurring in these catchments. This finding complements previous work and provides valuable evidence concerning the Mackenzie organic matter quality which is depleted in humic material as reported previously during summer time; this depletion is attributed to (i) a long freshwater residence time in Mackenzie catchments (Retamal et al., 2007), (ii) a preferential sorption of the high molecular weight hydrophobic DOM components to abundant suspended sediments (Stedmon et al., 2011) and (iii) a more extensive photodegradation of the high molecular weight fraction occurring in the Mackenzie watershed during summer (Osburn et al., 2009).

4 Conclusions

In this study, the specific absorbance (a_{CDOM} (350)) and the magnitude of CDOM in the Mackenzie Delta sector (salinity < 15) were significantly higher than those observed in the saltiest waters (salinity > 25) while the values for the intermediate salinity sector (15 < salinity < 25) were characteristic of a DOM transition zone. Surface CDOM, that could be considered the dominant attenuator of UV-A and PAR radiation, was a good proxy for DOC in both the Mackenzie dilution plume area (salinity < 25 conservative behavior) and in the saltiest waters (salinity > 25; in situ DOM production coupled with

BGD
9, 15567–15602, 2012

a limited DOM photodegradation process). Despite S_{CDOM} values being similar across the different surface salinity sectors, two distinct origins of the absorbent DOM content were observed throughout this system. The reactive allochthonous DOM dominated only in the Mackenzie Delta sector (salinity < 15) and the autochthonous DOM was prevalent in the North East sector (salinity > 25).

The EEM composition was surprisingly dominated by both biological components through the system. The spatial distribution of the protein-like component C3 was relatively homogeneous throughout the system except at specific off shore stations where processes leading to its in situ production occurred. In contrast, the overall distribution of the terrestrial component C2 appeared was restricted to the Mackenzie Delta sector and paralleled exactly the highly absorbing allochthonous CDOM observed. The surface distribution of the in-situ biological component C1 appeared more widespread than the terrestrial component C2 throughout the system, most likely due to the ubiquitous nature of its formation. However, it is clear and surprising that the strongest C1 signature was observed in the Mackenzie Delta sector. This in-situ biological component probably originates from the important phytoplanktonic and macrophytic activity (Squires et al., 2009) occurring in the open waters of the Mackenzie's freshwater catchment prior its marine discharge.

This finding provides valuable information concerning the Mackenzie River's organic matter quality which appears to be depleted in humic terrestrial materials as noted previously during summer, this depletion is attributed to (i) a high freshwater residence time in Mackenzie catchments (Retamal et al., 2007), (ii) a preferential adsorption of the high molecular hydrophobic DOM components to abundant suspended sediments (Stedmon et al., 2011) and (iii) a more extensive photodegradation of the high molecular weight fraction occurring in the vast Mackenzie watershed during the summer period (Osburn et al., 2009). Moreover, these statements taken as a whole will help explain the large proportion of autochthonous CDOM recently evidenced in surface waters of the Canadian Basin (Stedmon et al., 2011) compared to the more riverine findings for the Eurasian Basin. Therefore, the apparent autochthonous CDOM evolution in surface

BGD
9, 15567–15602, 2012

waters of the Canadian Basin may be the result of a biological CDOM mixture produced either in the watershed (terrestrial) and in-situ.

Acknowledgements. This study was conducted as part of the Malina Scientific Program funded by ANR (Agence nationale de la recherche), INSU-CNRS (Institut national des sciences de l'Univers – Centre national de la recherche scientifique), CNES (Centre national d'études spatiales) and ESA (European Space Agency). We are grateful to M. Babin PI of the Malina Project as well as the captain and crews of the Canadian Icebreaker CCGS Amundsen. We also thank S. Belanger, A. Mucci, B. Lansard and C. Stedmon for SIM/Chl *a* data and PARAFAC analysis. Special thanks are due to C. Marec and Y. Graton for water sampling. We are grateful to Marc Tedetti and Madeleine Goutx for their help for fluorescence analyse. R. Sempere acknowledges funding from Conseil général des Bouches du Rhône. PhD scholarship to J. Para was provided by the Region of Provence Alpes Côte d'Azur and AtmoPACA.

The publication of this article is financed by CNRS-INSU.

References

Babin, M., Stramski, D., Ferrari, G. M., Claustre, H., Bricaud, A., Obolensky, G., and Hoepffner, N.: Variations in the light absorption coefficients of phytoplankton, nonalgal particles, and dissolved organic matter in coastal waters around Europe, J. Geophys. Res., 108, 1–20, doi:10.1029/2001JC000882, 2003.

Baker, K. S. and Smith, R. C.: Bio-optical classification and model of natural waters, Limnol. Oceanogr., 27, 500–509, 1982.

BGD

9, 15567–15602, 2012

Barber, D. G. and Hanesiak, J.: Meteorological forcing of sea ice concentrations in the Southern Beaufort Sea over the period 1978 to 2001, J. Geophys. Res., 109, C06014, doi:10.1029/2003JC00202, 2004.
Belzile, C., Vincent, W. F., and Kumagai, M.: Contribution of absorption and scattering to the attenuation of UV and photosynthetically available radiation in Lake Biwa, Limnol. Oceanogr., 47, 95–107, doi:10.1029/2003JC002027, 2002.
Belzile, C., Roesler, C. S., Christensen, J. P., Shakhova, N., and Semiletov, I.: Fluorescence measured using the WETStar DOM fluorometer as a proxy for dissolved matter absorption, Estuar. Coast. Shelf S., 67, 441–449, 2006.
Carmack, E. C. and Macdonald, R. W.: Oceanography of the Canadian shelf of the Beaufort Sea: a setting for marine life, Arctic, 55 (Suppl. 1), 29–45, 2002.
Coble, P. G.: Characterization of marine and terrestrial DOM in seawater using excitation emission matrix spectroscopy, Mar. Chem., 51, 325–346, 1996.
Coble, P. G., Schultz, C. A., and Mopper, K.: Fluorescence contouring analysis of DOC intercalibration experiments samples: a comparison of techniques, Mar. Chem., 41, 173–178, 1993.
Coble, P. G., Del Castillo, C. E., and Avril, B.: Distribution and optical properties of CDOM in the Arabian Sea during the 1995 southwest monsoon, Deep-Sea Res., II, 45, 2195–2223, 1998.
Dittmar, T. and Kattner, G.: The biogeochemistry of the river and shelf ecosystem of the Arctic Ocean, a review, Mar. Chem., 83, 103–120, 2003.
Emmerton, C. A., Lesack, L. F. W., and Marsh, P.: Lake abundance, potential water storage, and habitat distribution in the Mackenzie River Delta, western Canadian Arctic, Water Resour. Res., 43, W05419, doi:10.1029/2006WR005139, 2007.
Emmerton, C. A., Lesack, L. F. W., and Vincent, W. F.: Mackenzie River nutrient delivery to the Arctic Ocean and effects of the Mackenzie Delta during open water conditions, Glob. Biogeochem. Cycles, 22, GB1024, doi:10.1029/2006GB002856, 2008.
Fellman, J. B., Spencer, R. G. M., Hernes, P. J., Edwards, R. T., D'Amore, D. V., and Hood, E.: The impacts of glacier runoff on the biodegradability and biochemical composition of terrigenous dissolved organic matter in near-shore marine ecosystems, Mar. Chem., 121, 112–122, 2010.
Foley, J. A.: Tipping points in the tundra, Science, 310, 627–628, 2005.

BGD
9, 15567–15602, 2012

Gareis, J. A. L., Lesack, L. F. W., and Bothwell, M. L.: Attenuation of in situ UV radiation in Mackenzie Delta lakes with varying dissolved organic matter compositions, Water Resour. Res., 46, W09516, doi:10.1029/2009WR008747, 2010.

Gordeev, V. V.: Fluvial sediment flux to the Arctic Ocean, Geomorphology, 80, 94–104, doi:10.1016/j.geomorph.2005.09.008, 2006.

Guéguen, C., Guo, L., Yamamoto-Kawai, M., and Tanaka, N.: Colored dissolved organic matter dynamics across the shelf-basin interface in the western Arctic Ocean, J. Geophys. Res., 112, C05038, doi:10.1029/2006JC003584, 2007.

Guo, L., Ping, C. L., and Macdonald, R. W.: Mobilization pathways of organic carbon from permafrost to arctic rivers in a changing climate, Geophys. Res. Lett., 34, L13603, doi:10.1029/2007GL030689, 2007.

IPCC Climate Change: The Physical Science Basis: Contribution of Working Group I to the Fourth Assessment Report of the IPCC, Cambridge University, Cambridge, 7, 514–515, 2007.

Jin, Z., Charlock, T., Smith Jr., W., and Rutledge, K.: A parameterization of ocean surface albedo, Geophys. Res. Lett., 31, L22301, doi:10.1029/2004GL021180, 2004.

Johannessen, S. C. and Miller, W. L.: Quantum yield for the photochemical production of dissolved inorganic carbon in seawater, Mar. Chem., 76, 271–283, 2001.

Lawrence, D. M. and Slater, A. G.: A projection of severe nearsurface permafrost degradation during the 21st century, Geophys. Res. Lett., 32, L24401, doi:10.1029/2005GL025080, 2005.

Macdonald, R. W., Solomon, S. M., Cranston, R. E., Welch, H. E., Yunker, M. B., and Gobeil, C.: A sediment and organic carbon budget for the Canadian Beaufort, Sea. Mar. Geol., 144, 255–273, 1998.

Matsuoka, A., Hill, V., Huot, Y., Bricaud, A., and Babin, M.: Seasonal variability in the light absorption properties of western Arctic waters: parameterization of the individual components of absorption for ocean color applications, J. Geophys. Res., 116, 8, 11003–11040, doi:10.1029/2009JC005594, 2011.

Matsuoka, A., Bricaud, A., Benner, R., Para, J., Sempéré, R., Prieur, L., Bélanger, S., and Babin, M.: Tracing the transport of colored dissolved organic matter in water masses of the Southern Beaufort Sea: relationship with hydrographic characteristics, Biogeosciences, 9, 925–940, doi:10.5194/bg-9-925-2012, 2012.

BGD
9, 15567–15602, 2012

Mucci, A., Lansard, B., Miller, L. A., and Papakyriakou, T. N.: CO_2 fluxes across the air-sea interface in the southeastern Beaufort Sea: Ice-free period, J. Geophys. Res., 115, C04003, doi:10.1029/2009JC005330, 2010.
Mueller, J. L. and Austin, R. W.: Ocean Optics Protocols for SeaWiFS Validation, Revision 1. NASA Tech. Memo. 104566, edited by: Hooker, S. B., Firestone, E. R., and Acker, J. G., NASA GSFC, Greenbelt, Maryland, 25, 67 pp., 1995.
Nagata, T.: Production mechanisms of Dissolved Organic Matter, in: Microbial Ecology of the Oceans, edited by: Kirchman, D. L., Wiley-Liss, New York, 5, 121–152, 2000.
Nelson, N. B., Carlson, C. A., and Steinberg, D. K.: Production of chromophoric dissolved organic matter by Sargasso Sea microbes, Mar. Chem., 89, 273–287, 2004.
O'Brien, M. C., Macdonald, R. W., Melling, H., and Iseki, K.: Particle fluxes and geochemistry on the Canadian Beaufort Shelf: implications for sediment transport and deposition, Cont. Shelf Res., 26, 41–81, 2006.
Opsahl, S., Benner, R., and Amon, R.: Major flux of terrigenous dissolved organic matter through the Arctic Ocean, Limnol. Oceanogr., 44, 2017–2023, 1999.
Osburn, C. L., O'Sullivan, D. W., and Boyd, T. J.: Increases in the longwave photobleaching of chromophoric dissolved organic matter in coastal waters, Limnol. Oceanogr., 54, 145–159, 2009.
Para, J., Coble, P. G., Charrière, B., Tedetti, M., Fontana, C., and Sempéré, R.: Fluorescence and absorption properties of chromophoric dissolved organic matter (CDOM) in coastal surface waters of the northwestern Mediterranean Sea, influence of the Rhône River, Biogeosciences, 7, 4083–4103, doi:10.5194/bg-7-4083-2010, 2010.
Raymond, P. A., McClelland, J. W., Holmes, R. M., and Zhulidov, A. V.: Flux and age of dissolved organic carbon exported to the Arctic Ocean: A carbon isotopic study of the five largest Arctic rivers, Global Biogeochem. Cycles, 21, GB4011, doi:10.1029/2007GB002934, 2007.
Retamal, L., Vincent, W. F., Martineau, C., and Osburn, C. L.: Comparison of the optical properties of dissolved organic matter in two river in?uenced coastal regions of the Canadian Arctic, Estuar. Coast. Shelf Sci., 72, 261–272, 2007.
Retamal, L., Bonilla, S., and Vincent, W. F.: Optical gradients and phytoplankton production in the Mackenzie River and the coastal Beaufort Sea, Polar Biol., 31, 363–379, 2008.
Sempéré, R., Tedetti, M., Panagiotopoulos, C., Charrière, B., and Van Wambeke, F.: Distribution and bacterial availability of dissolved neutral sugars in the South East Pacific, Biogeosciences, 5, 1165–1173, doi:10.5194/bg-5-1165-2008, 2008.

BGD
9, 15567–15602, 2012

Smith, R. C. and Baker, K. S.: The analysis of ocean optical data, Proceedings of The Society of Photo-Optical Instrumentation Engineers, Ocean Optics VII, 489, 119–126, 1984.
Sohrin, R. and Sempéré, R.: Seasonal variation in total organic carbon in the Northeast Atlantic in 2000–2001, J. Geophys. Res., 110, C10S90, doi:10.1029/2004JC002731, 2005.
Squires, M. M., Lesack, L. F. W., Hecky, R. E., Guildford, S. J., Ramlal, P., and Higgins, S. N.: Primary Production and Carbon Dioxide Metabolic Balance of a Lake-Rich Arctic River Floodplain: Partitioning of Phytoplankton, Epipelon, Macrophyte, and Epiphyton Production Among Lakes of the Mackenzie Delta, Ecosystems, 12, 853–872, doi:10.1007/s10021-009-9263-3, 2009.
Stedmon, C. A. and Bro, R.: Characterizing dissolved organic matter fluorescence with parallel factor analysis, a tutorial, Limnol. Oceanogr. Methods, 6, 572–579, 2008.
Stedmon, C. A. and Markager, S.: Tracing the production and degradation of autochthonous fractions of dissolved organic matter using fluorescence analysis, Limnol. Oceanogr., 50, 1415–1426, 2005.
Stedmon, C. A., Markager, S., and Bro, R.: Tracing dissolved organic matter in aquatic environments using a new approach to fluorescence spectroscopy, Mar. Chem., 82, 239–254, doi:10.1016/S0304-4203(03)00072-0, 2003.
Stedmon, C. A., Thomas, D. N., Granskog, M., Kaartokallio, H., Papadimitriou, S., and Kuosa, H.: Characteristics of dissolved organic matter in Baltic coastal sea ice: allochthonous or autochthonous origins?, Environ. Sci. Technol., 41, 7273–7279, 2007.
Stedmon, C. A., Amon, R. M. W., Rinehart, A. J., and Walker, S. A.: The supply and characteristics of colored dissolved organic matter (CDOM) in the Arctic Ocean: Pan Arctic trends and differences, Mar. Chem., 124, 108–118, 2011.
Tarnocai, C., Canadell, J. G., Schuur, E. A. G., Kuhry, P., Mazhitova, G., and Zimov, S.: Soil organic carbon pools in the northern circumpolar permafrost region, Glob. Biogeochem. Cycles, 23, GB2023, doi:10.1029/2008GB003327, 2009.
Tedetti, M. and Sempéré, R.: Penetration of Ultraviolet Radiation in the Marine Environment, a Review, Photochem. Photobiol., 82, 389–397, 2006.
Tedetti, M., Sempéré, R., Vasilkov, A., Charrière, B., Nérini, D., Miller, W.L., Kawamura, K., Raimbault, P.: High penetration of ultraviolet radiation in the south east Pacific waters, Geophys. Res. Lett., 34, L12610, doi:10.1029/2007GL029823, 2007.

BGD
9, 15567–15602, 2012

Tedetti, M., Guigue, C., and Goutx, M.: Utilization of a submersible UV fluorometer for monitoring anthropogenic inputs in the Mediterranean coastal waters, Mar. Pollut. Bull., 60, 350–362, 2010.

Walker, S. A., Amon, R. M. W., Stedmon, C., Duan, S., and Louchouarn, P.: The use of PARAFAC modeling to trace terrestrial dissolved organic matter and fingerprint water masses in coastal Canadian Arctic surface waters, J. Geophys. Res., 114, G00F06, doi:10.1029/2009JG000990, 2009.

Walvoord, M. A. and Striegl, R. G.: Increased groundwater to stream discharge from permafrost thawing in the Yukon River basin: potential impacts on lateral export of carbon and nitrogen, Geophys. Res. Lett., 34, L12402, doi:10.1029/2007GL030216, 2007.

Yamashita, Y. and Tanoue, E.: Chemical characterization of protein-like fluorophores in DOM in relation to aromatic amino acids, Mar. Chem., 82, 255–271, 2003.

Zhang, Y., van Dijk, M. A., Liu, M., Zhu, G., and Qin, B.: The contribution of phytoplankton degradation to chromophoric dissolved organic matter (CDOM) in eutrophic shallow lakes: field and experimental evidence, Water. Res., 43, 4685–4697, 2009.

BGD

9, 15567–15602, 2012

Table 1. Bottom depth, temperature, salinity, DOC and absorbance properties, including CDOM absorption coefficient, spectral slope and the specific absorption coefficient at 350 nm(a_{CDOM}*(350) determined in surface waters of each sampling stations and among the different sectors investigated (i.e. North East, North West and Mackenzie Delta sectors) observed.

Station	Bottom depth (m)	Temperature (°C)	Salinity	DOC (µM)	a_{CDOM} (350) (m^{-1})	a_{CDOM}*(350) (m^2 µmol^{-1})	S_{CDOM} (nm^{-1})
North East sector							
150	65	3.55	29.41	83.6	0.29	3.51	0.020
170	37	3.19	29.37	114.7	0.56	4.89	0.018
260	59	4.61	29.26	79.9	0.19	2.32	0.019
110	407	4.36	28.93	75.2	0.14	1.89	0.019
240	475	3.23	28.90	61.9			
130	310	4.63	28.22	67.5	0.17	2.53	0.019
135	227	2.24	28.05	67	0.15	2.19	0.020
380	62	4.41	27.67	74.2	0.21	2.88	0.019
280	41	4.71	27.63	89.3	0.38	4.21	0.019
223	940	−0.07	27.54	65.7	0.15	2.31	0.019
345	586	1.96	27.49	62	0.12	1.95	0.020
340	559	0.13	26.87	61.1	0.13	2.09	0.020
320	1134	−0.78	26.52	58.4	0.13	2.28	0.019
360	76	−0.17	26.47	61.9	0.12	2.01	0.021
540	1511	−0.41	25.73	61.4	0.16	2.60	0.023
430	1282	−0.78	25.96	59.2	0.14	2.37	0.022
460	357	−0.09	24.78	58.1	0.19	3.26	0.021
Mean	*478*	*2.04*	*27.58*	*70.6*	*0.20*	*2.71*	*0.020*
SD	*471*	*2.18*	*1.38*	*14.7*	*0.12*	*0.86*	*0.001*
North West sector							
760	543	0.54	22.52	73.4	0.43	5.80	0.019
620	1541	2.07	22.06	93.7	0.77	8.20	0.019
660	259	4.25	21.90	104.3	0.77	7.38	0.019
670	124	5.39	21.86	105.2			
394	11	8.81	21.45	199.7	2.28	11.42	0.017
780	49	4.10	21.08	110.3	0.77	6.97	0.019
Mean	*421*	*4.19*	*21.81*	*114.4*	*1.00*	*7.95*	*0.019*
SD	*581*	*2.85*	*0.50*	*43.8*	*0.73*	*2.12*	*0.001*
Mackenzie Delta sector							
680	121	8.05	14.76	118.5	2.35	12.49	0.018
694	11	9.28	9.43	316.3	5.05	15.96	0.019
695	4	9.56	7.56	341.7	5.60	16.39	0.019
696	3	10.08	0.23	394.2	6.36	16.13	0.020
Mean	*35*	*9.24*	*8.00*	*292.9*	*4.84*	*15.24*	*0.019*
SD	*58*	*0.86*	*6.01*	*120.5*	*1.74*	*1.84*	*0.001*

BGD
9, 15567–15602, 2012

Table 2. Values of diffuse attenuation coefficient of light in the UV-B (305 nm), UV-A (325, 340 and 380 nm) and PAR spectral domains determined in surface waters of each sampling stations and among the different sectors. Environmental conditions, including SZA, wind speed, cloud optical depth estimation are also reported as well as the maximal depth range from which surface $K_d(\lambda)$ values were derived.

Station	SZA (Deg.)	Wind speed (ms-1)	Cloud optical depth	Depth range (m)	Kd (305 nm) (ms-1)	Kd (325 nm) (ms-1)	Kd (340 nm) (ms-1)	Kd (380 nm) (ms-1)	Kd (PAR) (ms-1)
North East sector									
150	71	13	20	0–10	–	0.477	0.367	0.199	0.101
170	56	5	20	0–7	–	1.135	0.959	1.582	0.235
260	58	2	5	0–30	0.461	0.403	0.304	0.159	0.088
110	56	13	15	0–30	0.448	0.346	0.260	0.129	0.076
240	68	9	15	0–30	–	0.342	0.257	0.129	0.071
135	59	9	10	0–30	0.359	0.352	0.135	0.070	
380	66	3	10	0–6	–	0.635	0.495	0.241	0.093
345	58	3	15	0–30	0.366	0.296	0.111		
360	57	4	10	0–30	0.306	0.283	0.229	0.117	0.063
540	58	3	10	0–30	0.361	0.316	0.241	0.112	0.064
460	66	5	5	0–30	0.360	0.337	0.266	0.127	0.070
Mean					*0.380*	*0.447*	*0.351*	*0.276*	*0.091*
SD					*0.055*	*0.249*	*0.216*	*0.458*	*0.049*
North West sector									
760	62	2	10	0–8	–	0.790	0.620	0.298	0.100
620	66	3	5	0–5	–	1.135	0.927	0.423	0.122
660	79	4	5	0–8	–	–	0.999	0.609	0.146
670	55	7	5	0–5	–	1.641	1.414	0.615	0.163
780	80	2	10	0–6	–	1.504	1.316	0.616	0.150
Mean						*1.268*	*1.055*	*0.512*	*0.136*
SD						*0.383*	*0.318*	*0.145*	*0.025*

BGD
9, 15567–15602, 2012

Table 3. Spectral characteristics of the three components identified by PARAFAC analysis compared to previously identified components including Arctic and sub-Arctic studies (Stedmon et al., 2007; Walker et al., 2009; Fellman et al., 2010). Position of Ex/Em maxima of C1, C2 and C3 are deduced from their corresponding spectra reported in Fig. 8.

	Components		
	C1	C2	C3
Ex. Maxima (nm)	< 240 (300)	< 240 (340)	< 240 (275)
Em. Maxima (nm)	404	472	314
Coble et al. (1998)	M	A and C	B and T
Stedmon et al. (2007)	C3	C1	C4 and C5
Walker et al. (2009)	BERC6	BERC3	BERC5
Fellman et al. (2010)	C5	CA and (C2)	C8 and C7
Source	Marine and Terrestrial	Terrestrial (allochtonous)	Amino acids (allochtonous)

BGD
9, 15567–15602, 2012

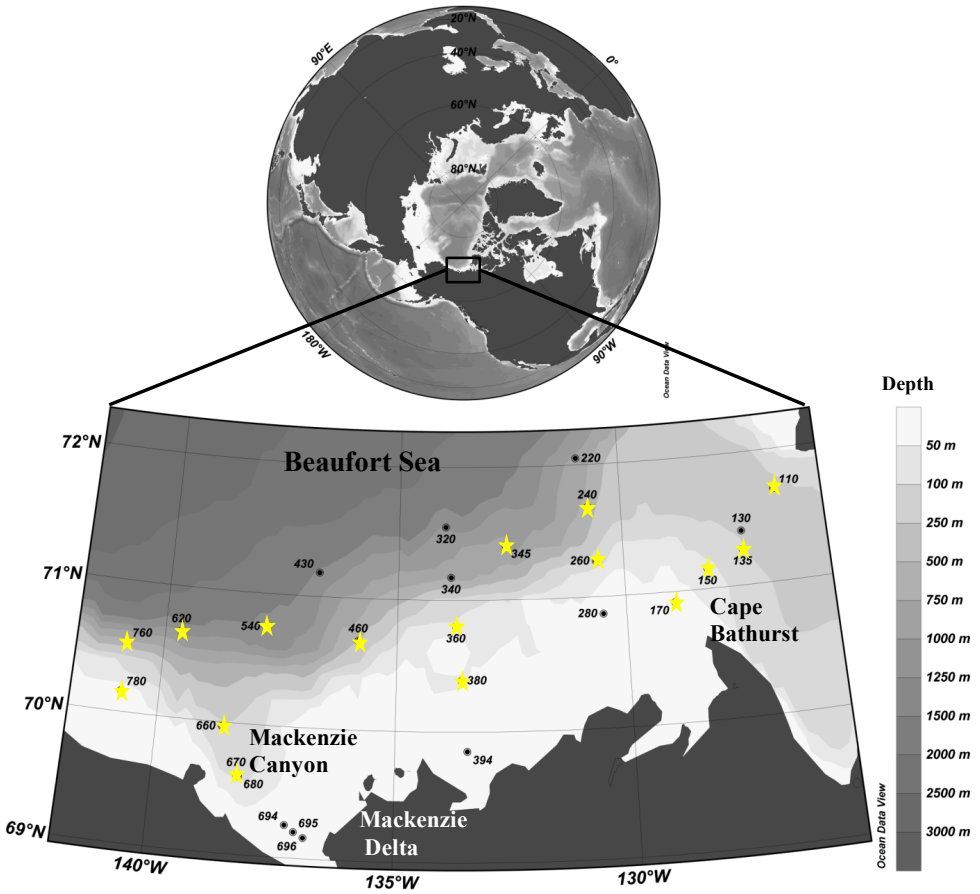

Fig. 1. Location and station number investigated during the MALINA cruise in the Canadian Shelf of the Beaufort Sea. Yellow stars represent the stations where profiles of downward irradiance were performed.

BGD
9, 15567–15602, 2012

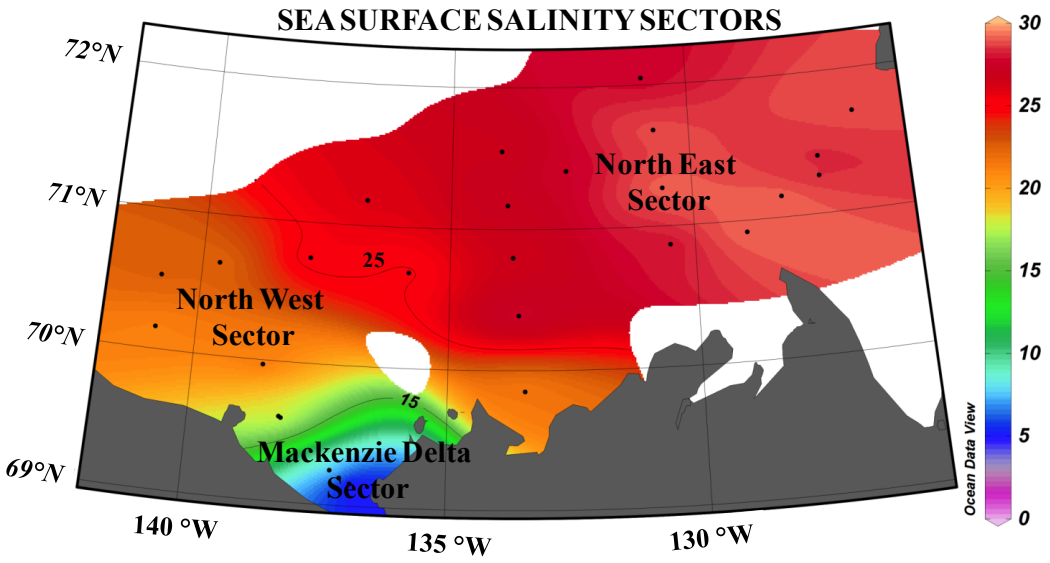

Fig. 2. Map of the sea surface salinity illustrating the different surface salinity sectors observed during the study: Mackenzie Delta sector (salinity < 15), North West sector (15 < salinity < 25) and North East sector (salinity > 25). Isohalines 15 and 25 mark the boundaries of these sectors.

BGD
9, 15567–15602, 2012

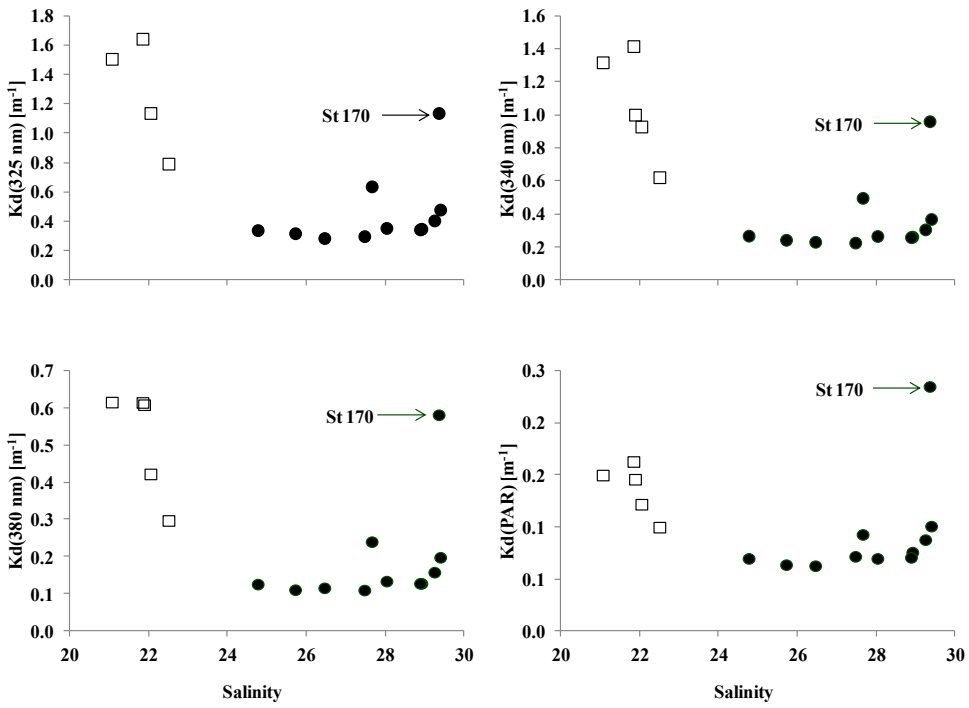

Fig. 3. Diffuse attenuation coefficient of light (K_d) at 325, 340, 380 nmand PAR as a function of surface salinity in the North East (circles) and North West (squares) sectors. Station 170 was characterized by high DOC (117 µM), Chlorophyll *a* (~ 7 µg l^{-1}) and a_{CDOM} (350 nm) (0.56 m^{-1}) content.

BGD
9, 15567–15602, 2012

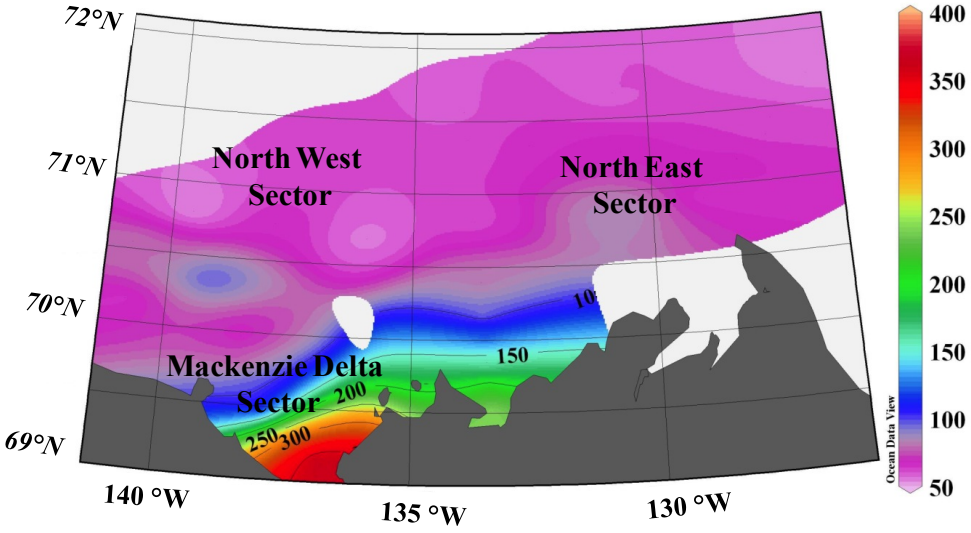

Fig. 4. Map of the surface DOC (μM) distribution in Beaufort Sea during the MALINA cruise.

BGD
9, 15567–15602, 2012

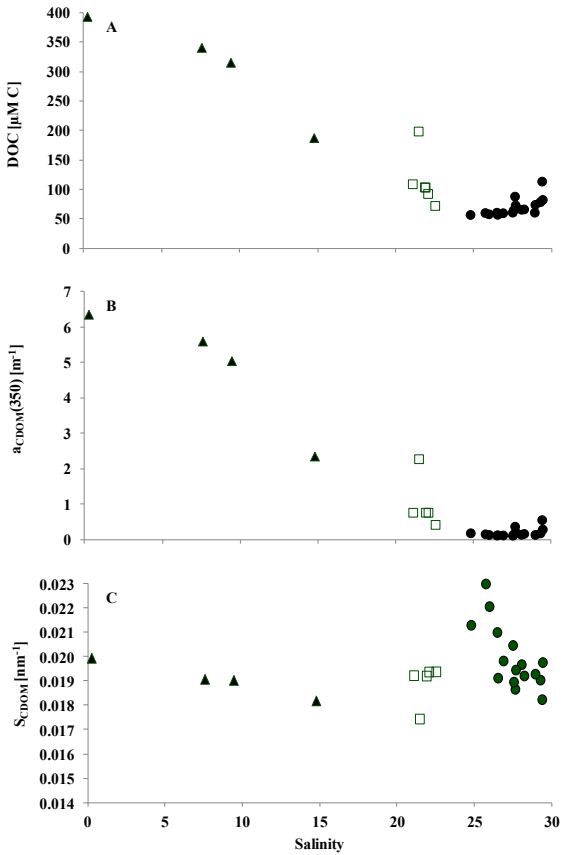

Fig. 5. Dissolved organic carbon (DOC) **(A)**, absorption coefficient at 350 nm(a_{CDOM} (350)) **(B)** and spectral slope (S_{CDOM}) **(C)** as a function of surface salinity in the North East (circles), North West (squares) and Mackenzie Delta (triangles) sectors.

BGD
9, 15567–15602, 2012

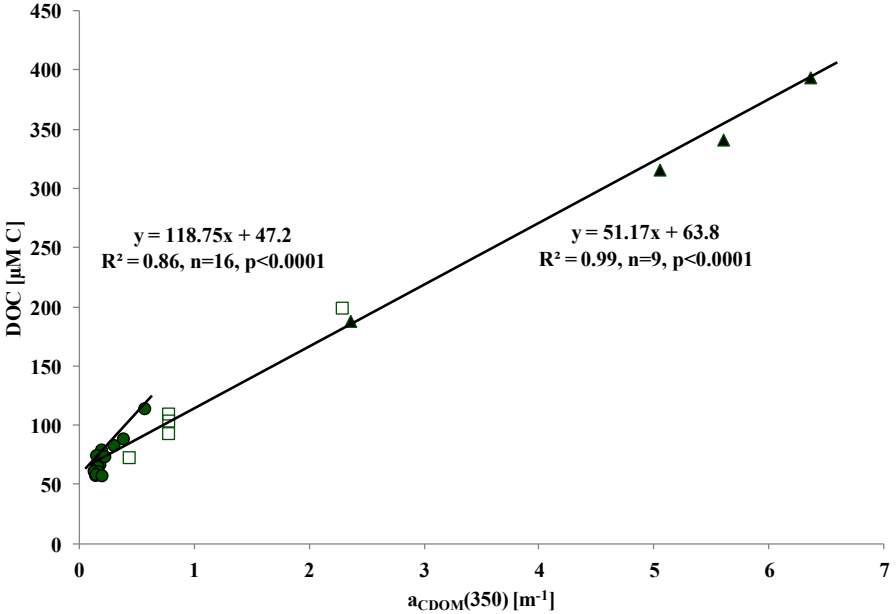

Fig. 6. Relationships observed between dissolved organic carbon (DOC) concentration and absorption coefficient of CDOM at 350 nm ($a_{CDOM}(350)$) determined in the Mackenzie Delta and North West sectors (salinity < 25, triangles and squares) and in the North East sector (salinity > 25, circles).

BGD
9, 15567–15602, 2012

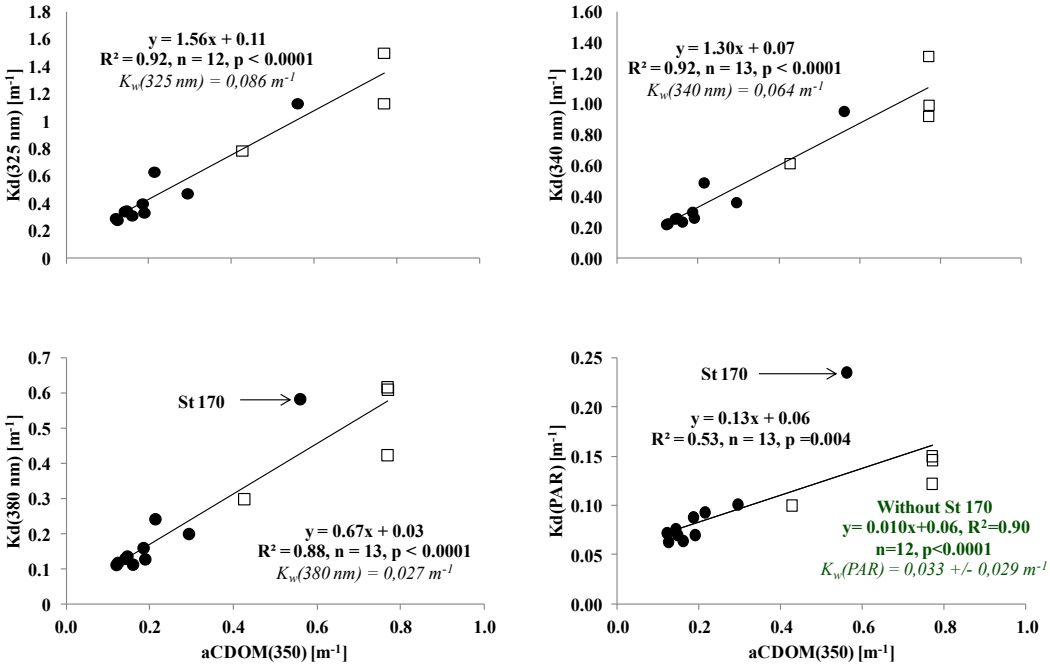

Fig. 7. Relationships between surface diffuse attenuation coefficient of light (K_d) determined in the UVR-A (325, 340 and 380 nm) and PAR spectral domains with absorption coefficient of CDOM at 350 nm (a_{CDOM} (350)) observed in the two saltiest surface salinity sectors [North West (squares) and North East sectors (circles)]. K_w = diffuse attenuation coefficient values for pure water (K_w (λ)) determined by Baker and Smith (1982).

BGD
9, 15567–15602, 2012

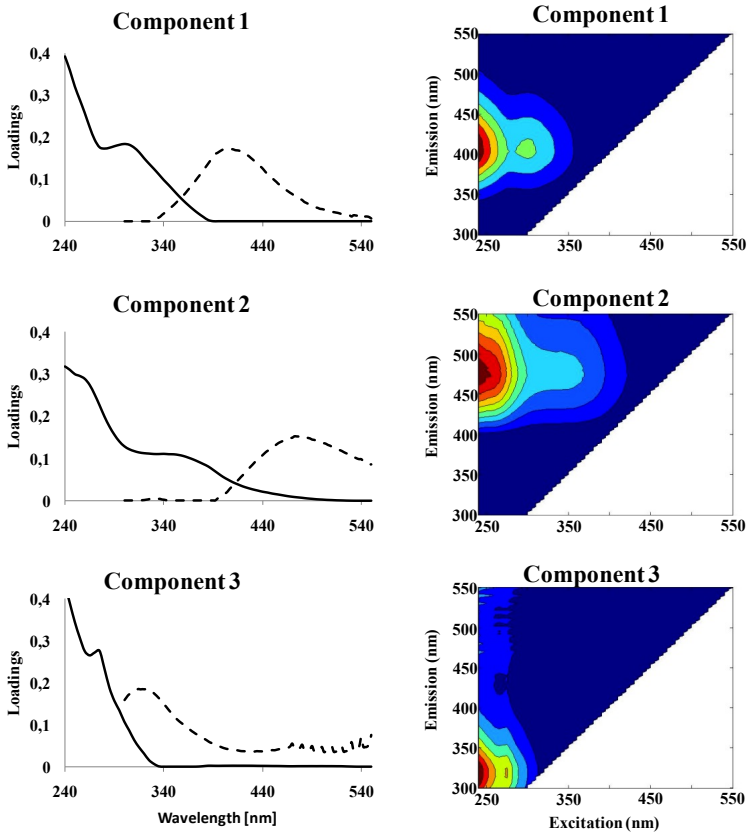

Fig. 8. Emission (dashed line) and Excitation (solid line) spectra (left panels) and contour plots (right panels) of the three main fluorescent components identified in the dataset (n = 54). Ex/Em Component 1: 240 (300)/404; Ex/Em Component 2: 240 340)/472 and Ex/Em Component 3: 240 (275)/314.

BGD
9, 15567–15602, 2012

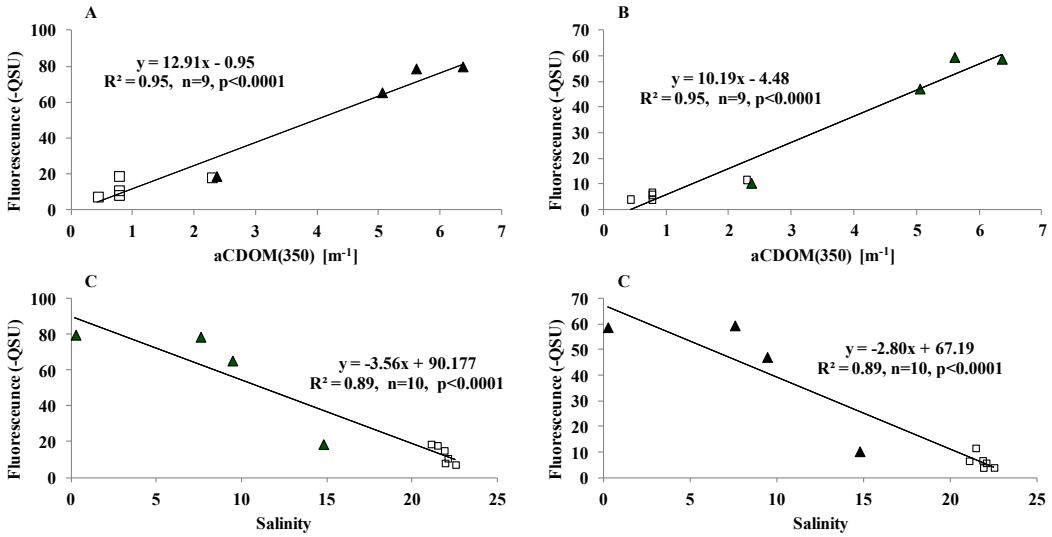

Fig. 9. Relationships observed between C1 **(A, B)** and C2 **(C, D)** components with absorption coefficient of CDOM at 350 nm [a_{CDOM} (350)] and salinity determined in the Mackenzie Delta (triangles) and North West sectors (squares).

BGD
9, 15567–15602, 2012

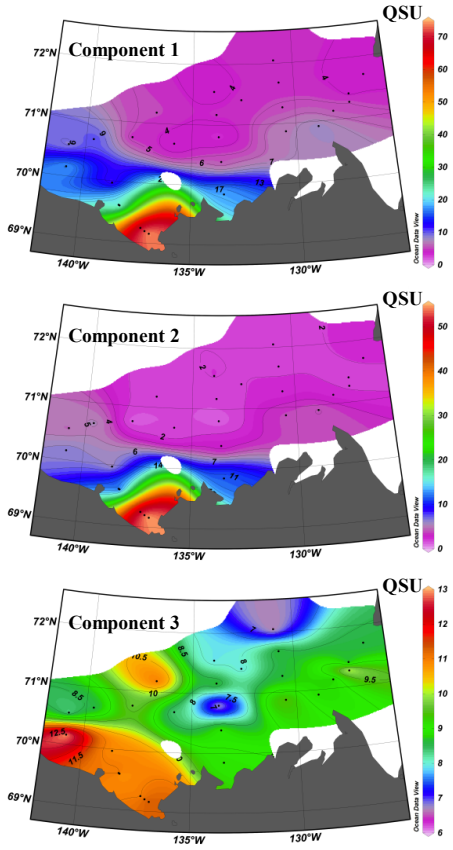

Fig. 10. Spatial distribution of fluorescence intensity (QSU) of the component 1, 2 and 3 identified in surface waters of the Canadian Shelf in the Beaufort Sea.

BGD
9, 15567–15602, 2012